Olig1 and *Olig2* triplication causes developmental brain defects in Down syndrome

Lina Chakrabarti[1], **Tyler K. Best**[2], **Nathan P. Cramer**[2], **Rosalind S.E. Carney**[1], **John T.R. Isaac**[3], **Zygmunt Galdzicki**[2], and **Tarik F. Haydar**[1],[€]

[1] Center for Neuroscience Research, Children's National Medical Center, Washington DC, 20010

[2] Department of Anatomy, Physiology and Genetics, School of Medicine, Uniformed Services University of the Health Sciences, Bethesda, Maryland 20814

[3] Developmental Synaptic Plasticity Section, NINDS, Bethesda, MD 20892

Summary

Over-inhibition is thought to be one of the underlying causes of the cognitive deficits in Ts65Dn mice, the most widely used model of Down syndrome (DS). Here we demonstrate a direct link between gene triplication and defects in neuron production during embryonic development. These neurogenesis defects lead to an imbalance between excitatory and inhibitory neurons and to increased inhibitory drive in the Ts65Dn forebrain. We discovered that *Olig1* and *Olig2*, two genes triplicated in DS and Ts65Dn, are over-expressed in the Ts65Dn forebrain. To test the hypothesis that *Olig* triplication is causative for the neurological phenotype, we used a genetic approach to normalize the dosage of these two genes and thereby rescued the inhibitory neuron phenotype in the Ts65Dn brain. These data identify seminal alterations during brain development and demonstrate a mechanistic relationship between triplicated genes and these brain abnormalities in the Ts65Dn mouse.

Keywords

cell density; Down syndrome; excitatory neurons; inhibitory neurons; *Olig1*; *Olig2*; Ts65Dn

Introduction

Down syndrome (DS), caused by triplication of chromosome 21, is the most frequent genetic cause of intellectual disability[1],[2]. Although the etiology of the cognitive deficit remains unclear, cellular and anatomical abnormalities in the prenatal and perinatal

forebrain and cerebellum suggest that early brain development is altered in DS[3]–[5]. Similar central nervous system (CNS) abnormalities have been described in mouse models of DS. In particular, the Ts65Dn mouse, the most widely used model of DS, has abnormal forebrain and cerebellar development[6]–[8], defects in synapse formation and neurophysiology[9]–[12] and behavioral deficits[13]–[15].

Recent studies have suggested that the major functional defect in the postnatal Ts65Dn brain may be an imbalance between excitation and inhibition. In addition to decreased numbers of excitatory synapses[10],[16] and relative increase in inhibitory synaptic markers in the cortex and hippocampus[9],[17], several groups have found that excessive GABA-mediated inhibition impairs the induction of long-term potentiation (LTP) in Ts65Dn hippocampus[10]–[12],[18]. A recent study also pointed to increased inhibition by showing that chronic treatment of Ts65Dn animals with GABA receptor antagonists could rescue defects in explicit learning, memory and LTP[19]. Altogether, these functional studies suggest that increased inhibitory synaptic drive may be a general physiological phenotype in the Ts65Dn forebrain. In this study, we sought to determine the molecular and cellular basis for this over-inhibition phenotype and therefore conducted a multidisciplinary series of experiments to assay neurophysiology, neurogenesis and the genetic mechanisms of altered growth of the Ts65Dn brain.

The mammalian forebrain is composed of two main classes of neurons, excitatory glutamatergic projection neurons and inhibitory GABAergic interneurons, both of which converge on the cortex through a diverse but precisely ordered sequence of developmental steps. Although they are generated from precursors in different telencephalic compartments, coordination in migration patterns, differentiation programs and network connectivity must occur between the projection neurons and interneurons for proper formation and function of the mature brain[20]–[22]. It is therefore possible that abnormalities in neuronal generation, migration or allocation may underlie the cognitive phenotype in DS. We recently discovered that embryonic neurogenesis in the dorsal neocortical ventricular zone (VZ) is transiently delayed in Ts65Dn mice[7], but how this delay affects postnatal cortical maturation, and whether the embryonic production of interneurons from their ventral telencephalic precursors was also affected were unknown.

Here, we demonstrate that a complex set of neurogenesis defects in multiple brain regions lead to an excitation/inhibition imbalance in the Ts65Dn forebrain. Furthermore, our studies implicate two genes triplicated in DS and Ts65Dn, *Olig1* and *Olig2*, in the defective ventral neurogenesis. Using an *in vivo* genetic normalization approach, we uncover a causal relationship between the extra gene dosage of *Olig1* and *Olig2* and the excitation/inhibition phenotype in the Ts65Dn forebrain.

Results

Neuronal allocation is impaired in Ts65Dn forebrain

First, to determine if the reduced embryonic neurogenesis in the dorsal neocortex we previously described[7] leads to a persistent paucity of excitatory neurons in Ts65Dn, we measured the density of T-brain1 (Tbr1^{+}) neurons in the pre- and postnatal Ts65Dn cortex.

We found, beginning in the first postnatal week (P8), that there were fewer Tbr1^{+} neurons in the Ts65Dn dorsal neocortex and that this paucity of excitatory neurons persisted at P15 and P30 (Supplementary Fig. 1 and Supplementary Table 1). Thus, the prenatal abnormalities in dorsal neocortical neurogenesis[7] result in long-lasting deficits in excitatory neuronal density in Ts65Dn neocortex.

To determine whether defects were also present in the inhibitory neuron lineage, we characterized the three major non-overlapping subclasses of forebrain interneurons (e.g. calretinin-, parvalbumin- and somatostatin- expressing groups). In contrast to the decreases in excitatory neurons, these studies revealed a profound increase in the number of parvalbumin[+] and somatostatin^{+} neurons in the Ts65Dn neocortex at P8, P15 and P30 (Fig. 1a,b, Supplementary Fig. 2 and Supplementary Table 1). Moreover, the number of cells expressing calbindin, a calcium-binding protein present in an overlapping population of interneurons[23–25] was also markedly increased in the Ts65Dn cortex (Fig. 1a,b, Supplementary Fig. 2 and Supplementary Table 1). Interestingly, though, no significant change was observed in the number of calretinin^{+} cells in Ts65Dn cortex at any of the ages studied. Supernumerary parvalbumin[+] and somatostatin^{+} cells were also found in the CA1 region of Ts65Dn hippocampus at P15 (+54% and +30% respectively) (Fig. 2) demonstrating a widespread over-abundance of interneurons throughout the Ts65Dn forebrain. These changes were confirmed by measurements of total calbindin protein content in the cortex (+43%) and hippocampus (+24%) of P15 Ts65Dn forebrain (Supplementary Fig. 2). Taken together, these results demonstrate a novel and significant overproduction of two specific classes of forebrain inhibitory neurons in Ts65Dn.

Increased inhibition in Ts65Dn forebrain

Although several reports have suggested that the defects in synaptic plasticity in Ts65Dn are due to over-inhibition[9–12], no data have directly demonstrated an inhibitory phenotype in Ts65Dn brain at the single cell level. We used patch-clamp recordings to measure the intrinsic membrane properties of forebrain neurons. We found that the rate of spontaneous inhibitory post-synaptic currents (sIPSC) is significantly higher (+300%) in CA1 pyramidal neurons from Ts65Dn compared to euploid mice (Supplementary Fig. 3a,c). This increased sIPSC frequency is consistent with larger number of interneurons since spontaneous action potential-mediated GABA release would naturally increase with more interneurons. To determine whether the increased sIPSC frequency was due to an increased number of interneurons or to a change in number of inhibitory terminals, we evaluated miniature IPSC (mIPSC). We found no significant difference in the frequency of mIPSC between euploid and Ts65Dn (Supplementary Fig. 3d. The increase in sIPSC frequency with no change in mIPSC indicates that although there are more interneurons, the number of inhibitory synapses per pyramidal neuron remains similar between euploid and Ts65Dn. Integration of these results therefore suggests that the interneurons are more active in the basal state in Ts65Dn hippocampus. To evaluate this possibility, we measured sIPSC under depolarizing conditions (9mM as opposed to 3 mM K^{+} ACSF) and found that the sIPSC frequency increased ~6 fold in euploid and only ~2 fold in Ts65Dn (Supplementary Fig. 3c) indicating that Ts65Dn interneurons are already shifted toward the upper range of excitability under basal conditions. Altogether, these studies indicate that the developmental overproduction of

Ts65Dn interneurons alters hippocampal circuitry such that interneurons spontaneously fire more frequently.

Effect of trisomy on gene triplication and neurogenesis

Next, we sought to understand the molecular reasons for the supernumerary interneurons in the Ts65Dn forebrain. It is now well-established that the vast majority of mouse forebrain interneurons are generated from precursors in the medial and caudal ganglionic eminences (MGE, CGE) of the ventral telencephalon[26]. These progenitor zones express a wide range of transcription factors including *Dlx 1/2/5/6*, *Nkx2-1* and *Lhx6,* all of which have critical roles in cell fate decisions and neuronal subtype specification[27]–[29]. Inhibitory neurons expressing parvalbumin and somatostatin primarily arise from the *Nkx2-1* and *Lhx6* expressing domain of the MGE while the calretinin-expressing interneurons are generated in the dorsal region of the CGE. Investigation of the neural precursor pools in the ganglionic eminences by *in situ* hybridization of *Dlx2, Dlx5, Nkx2-1* and *Lhx6*[30]–[33] demonstrate that *Lhx6*, which is preferentially expressed in postmitotic MGE cells, may be slightly expanded in Ts65Dn at E13.5 and E14.5 (Fig. 3a,b and Supplementary Fig. 4). Since *Lhx6* is required for interneuron specification, tangential migration and proper distribution in the cortical layers[28],[34], the increased numbers of interneurons in Ts65Dn cortex may be derived from an expanded population of *Lhx6*-expressing neuroblasts in the MGE.

Following on these gene expression studies, to determine whether the proliferation of the MGE progenitors are specifically affected in Ts65Dn, we assayed the rate of neuron production *in vivo*. Using a combination of pulse BrdU labeling and neuronal immuno-labeling by β-tubulin III (TUJ1) antibody (Fig. 3c), we measured the numbers of neurons produced from the ventral telencephalon within a 24 hr period. We found that the Ts65Dn MGE at E14.5 had 36% more BrdU$^+$/TUJ1$^+$ cells compared to euploid (Fig. 3d), indicating higher rates of neurogenesis in the Ts65Dn MGE. In contrast, consistent with the normal numbers of LGE- and CGE-derived neurons in the Ts65Dn telencephalon, the rates of neurogenesis in the LGE and CGE were statistically unchanged from controls (although LGE values demonstrated a possible trend). The increased production of TUJ1$^+$ cells in Ts65Dn MGE suggests higher output and potential depletion of MGE progenitors. Since premature depletion would be inconsistent with the findings of over-abundance of interneurons in the postnatal Ts65Dn neocortex, we measured the cell cycle duration of MGE cells at E13.5 and E14.5 to see whether cell division kinetics are different in the Ts65Dn MGE. We found that the labeling index (LI) slope and the time at which maximum LI is reached did not differ between euploid and Ts65Dn mice (Fig. 3e,f and Supplementary Table 2) suggesting that the length of the cell cycle is the same in both groups. However, these studies did indicate a larger proliferative cell population in the MGE of Ts65Dn brain at E13.5 and E14.5 (evident as a larger Y-intercept value). Moreover, the number of phosphohistone-3 (PH3) labeled M-phase cells was significantly increased in the SVZ of Ts65Dn MGE at both E14.5 and E15.5 (Fig. 3g,h). Taken together, these results suggest that a larger progenitor population in the VZ and SVZ of the Ts65Dn MGE undergoes divisions at a normal rate but with a higher neuronal output to generate supernumerary interneurons during the ventral neurogenesis period. These striking results uncover novel and highly specific regional defects in the neurogenesis pattern along the Ts65Dn dorsal-ventral axis

and elucidate the spatial and temporal underpinnings of the over-abundant interneuron population in the postnatal Ts65Dn cortex.

There are several transcription factor genes triplicated in DS and Ts65Dn which are known to be essential for specification of various cell types. For example, the basic helix-loop-helix (bHLH) transcription factors *Olig1* and *Olig2* are implicated in oligodendrogenesis and neurogenesis[35]–[37]. In particular, the expression pattern of *Olig2* in the MGE indicates a role in the generation of interneurons[38]–[40]. Because *Olig1* and *Olig2* are triplicated in DS and Ts65Dn, we reasoned that mis-expression of these genes may play a role in the Ts65Dn inhibition phenotype. Indeed, we detected a 1.7 and 1.5 fold increase in *Olig1* and *Olig2* expression, respectively, in the MGE of Ts65Dn brain at E14.5 using semiquantitative real time RT-PCR (Fig. 4e and Supplementary Table 3). In addition, more *Olig2*^{+} cells were found in the Ts65Dn MGE compared to euploid littermates at E13.5 and E14.5 (Fig. 4a–d,f). Previous studies which have shown that distinct cohorts of cortical interneurons arise from telencephalic *Olig2*-expressing precursors suggest that *Olig2* expression may be necessary for expression of several homeodomain containing genes in MGE, particularly *Lhx6*[40]. Therefore, these results suggest that *Olig1/Olig2* over-expression may be the genetic basis of the interneuron over-production in the Ts65Dn brain.

Olig normalization and rescue of the Ts65Dn phenotypes

To test the hypothesis that the extra *Olig1/Olig2* gene dosage is causally related to the MGE neurogenesis phenotype, we removed one allele of each gene within the Ts65Dn background by breeding Ts65Dn females with *Olig1/2*[+/−] double heterozygous males[37] (Fig. 4g). Quantification of *Olig2* expressing cells in the VZ and SVZ of the MGE of Ts65Dn*Olig1/2*[+/+/−] rescue animals at E14.5 revealed similar numbers of *Olig2* positive cells when compared to euploid animals (Supplementary Fig. 5). Furthermore, using the BrdU/TuJ1 method for measuring the rate of neurogenesis in the MGE of E14.5 Ts65Dn*Olig1/2*[+/+/−], full Ts65Dn, euploid and euploid*Olig1/2*[+/−] littermate pups, we found that returning Ts65Dn animals to disomy for just *Olig1* and *Olig2* was sufficient to reduce MGE neurogenesis to euploid levels (Fig. 4h). Furthermore, we used a BrdU and Ki67 double labeling paradigm to measure the fraction of cells leaving the cell cycle (the exiting fraction) in the MGE within a 24 hr period. As expected, we found that from E13.5 to E14.5 the exiting fraction was increased in the VZ (+36%) and SVZ (+31%) of Ts65Dn MGE, confirming the higher rates of neurogenesis in the Ts65Dn MGE. Importantly, the *Olig1/Olig2* gene dosage normalization rescued the exiting fraction in Ts65Dn*Olig1/2*[+/+/−] MGE to euploid control levels (Fig. 4 i,j). This *Olig1/Olig2* dosage reduction had a specific and major impact on MGE-derived cells during the prenatal period since *Lhx6* and somatostatin expressing cells were returned to normal numbers in the E15.5 ventral telencephalon in Ts65Dn*Olig1/2*[+/+/−] mice (Fig. 5a–h). Finally, to determine if this genetic rescue was sufficient to reverse the increased interneuron phenotype in the postnatal Ts65Dn brain, we measured the density of calbindin, parvalbumin and somatostatin expressing neurons in the Ts65Dn*Olig1/2*[+/+/−] cortical layers at P15. We found that the numbers of these interneuron subtypes in the *Olig1/Olig2* rescued mice were comparable to the euploid littermates (Fig. 6 and Supplementary Fig. 6 and Table 4). Altogether, these cellular, molecular and anatomical

studies establish the gene dosage imbalance for *Olig1* and *Olig2* as the underlying cause of the ventral neurogenesis and inhibitory neuron phenotype in Ts65Dn mice.

Lastly, to confirm that *Olig1/2* over-expression directly leads to the over-inhibition of pyramidal neurons in Ts65Dn forebrain, we assayed the electrophysiological characteristics of CA1 pyramidal neurons in Ts65Dn*Olig1/2*$^{+/+/−}$ rescue mutants. We found that the rate of sIPSC was significantly higher in Ts65Dn CA1 pyramidal neurons compared to euploid or Ts65Dn*Olig1/2*$^{+/+/−}$ littermates (Fig. 7a). Group data comparisons (n = 34, 27, and 33 cells for Ts65Dn, Ts65Dn*Olig1/2*$^{+/+/−}$, and euploid mice respectively) reveal a significant rightward shift in the frequency probability distribution function for Ts65Dn CA1 pyramidal cells (p < 0.001 vs. Ts65Dn*Olig1/2*$^{+/+/−}$ and euploid, one-way ANOVA with Tukey post-hoc comparison, Fig. 7b). Importantly, the sIPSC frequency distributions for Ts65Dn*Olig1/2*$^{+/+/−}$ and euploid littermates were not significantly different (p = 0.75), indicating that *Olig1/2* triplication leads to a higher activity of inhibitory inputs in Ts65Dn. Similar to our previous analysis (Supplementary Fig. 3), we found that the frequency of mIPSC were similar between euploid, Ts65Dn and Ts65Dn*Olig1/2*$^{+/+/−}$ neurons (Fig. 7c,d), indicating that while the Ts65Dn interneurons are more active, the number of synapses per pyramidal neuron is unchanged by trisomy. Taken together, these results demonstrate that reducing the *Olig1/2* gene dosage not only corrected the interneuron over-production phenotype in Ts65Dn but also rescued the excessive sIPSC frequency and over-inhibition of CA1 pyramidal cells in trisomic hippocampus.

Discussion

Our studies establish a link between prenatal neurogenesis defects and altered brain function in the postnatal Ts65Dn mouse, the most widely studied model of DS. To elucidate the molecular causes of this phenotype, we used a genetic rescue approach to show that increased gene dosage for *Olig1* and *Olig2* is responsible for the interneuron over-production. Deleting an allele of each of these genes prevented the interneuron over-production in the trisomic mouse brain. These data present the surprising result that increased gene dosage of just 2 of the 128 triplicated genes in Ts65Dn[41] are largely, if not solely, responsible for the interneuron phenotype in this mouse model.

For the first time, these results demonstrate that gene triplication can have quite opposite effects on cell proliferation in different regions of the developing brain. While only decreases in cell proliferation have thus far been found in DS fetal neocortex and fibroblasts[42,43] as well as in dorsal neocortical, cerebellar, and hippocampal precursor cells in Ts65Dn[7,42–44], the increased number of forebrain interneurons in Ts65Dn indicates that reduced proliferation is not a general hallmark of DS brain development. Rather, our results on transcription factor gene expression and precursor cell proliferation demonstrate that there is an increase in the number of Ts65Dn interneuron precursors which results in enhanced amplification of founder cells and greater neuronal output compared to the euploid. Thus, a diverse set of abnormalities, all of which are established during prenatal brain development, may combine to result in cognitive dysfunction in Ts65Dn mice.

The discovery of altered numbers of excitatory and inhibitory neurons may explain the electrophysiological abnormalities previously seen in adult Ts65Dn mice. A wide range of studies have explored the role of hippocampal function as the neurobiological basis for cognitive failure in Ts65Dn[10–12],[19]. One important hypothesis from these studies is that the suppression of LTP and augmentation of LTD in the Ts65Dn hippocampus is primarily due to enhanced inhibitory synaptic transmission. While others have found an increase in inhibitory synapse markers in the dentate gyrus of the Ts65Dn mouse[9], whether or not the number of inhibitory and excitatory neurons is changed during Ts65Dn development was unknown.

Here we find that an altered excitation/inhibition neuron ratio in Ts65Dn leads to over-inhibition of individual forebrain pyramidal neurons. In particular, not only is the number of inhibitory interneurons increased in Ts65Dn mice, but this change is accompanied by an increase in the rate and magnitude of IPSC inputs to CA1 pyramidal cells. The ability to reverse both phenotypes by decreasing the dosage of *Olig1/2* in trisomic mice supports a causal link between aberrant production of inhibitory interneurons and excessive inhibition in the hippocampus. The changes in frequency distribution of sIPSC without changes in mIPSC can be explained by an increase in action potential-dependent activity of interneurons. This could occur if intrinsic properties of interneurons are abnormal (lower action potential threshold) or by changes in the excitatory afferents activating the inhibitory network in the Ts65Dn hippocampus. For instance, since GABAergic interneurons directly receive all descending and intrahippocampal excitatory inputs[45], if excitatory input to the hippocampal feed-forward inhibitory network is diminished (e.g. due to the reductions in numbers of Ts65Dn forebrain excitatory neurons reported here) this could result in disinhibition of the inhibitory network in the Ts65Dn hippocampus.

In examining the intrinsic properties of CA1 pyramidal cells, we did not find any significant changes in resting membrane potential or membrane resistance between the groups. We did, however, find that the membrane capacitance was reduced in Ts65Dn and Ts65Dn*Olig1/2*[+/+/−] mice compared to euploid mice (Supplementary Figure 7 and Supplementary Table 5). This suggests that CA1 pyramidal cells in trisomic mice are smaller in size and possibly reflects reduced dendritic branching associated with trisomy[46]. Smaller dendritic trees presumably have less computational capacity which would be expected to exacerbate the aberrant processing of information resulting from over-inhibition.

These cellular and physiological data in the Ts65Dn telencephalon indicate that the balance between excitation and inhibition may be altered in DS and that this may underlie some or all of the cognitive deficits found in this prevalent disorder. Excitation-inhibition imbalance is now thought to be a major component of several other neurodevelopmental disorders including epilepsy, autism and Fragile X syndrome[47], [48]. It is also tempting to speculate that over-inhibition may be the basis of other abnormalities found in DS. For example, gene-dosage imbalance and over-inhibition may play a key role in the epileptic spasms in Ts65Dn mice, now considered a robust animal model of the infantile spasms occurring in DS[49]. In fact, gene triplication and increased expression of the G-protein coupled potassium channel (Girk2) is thought to underlie an increased $GABA_B$ receptor agonist contribution to hippocampal neuronal network activity as well as a potential role in induced epileptic

spasms in Ts65Dn mice[49],[50]. Therefore, inhibitory abnormalities may contribute to the prevalence of debilitating neurological disorders in DS children.

Our genetic rescue study has also potentially revealed a broader determinative role of *Olig1* and *Olig2* genes on ventral telencephalic neurogenesis. For example, we found that MGE neurogenesis in the ventral telencephalon and interneuron allocation to the postnatal neocortex was reduced in euploid *Olig1/2*$^{+/-}$ animals (Figs. 4h and 6, Supplementary Fig. 6 and Table 4). Thus, although it is well established that *Olig1* and *Olig2* regulate multiple steps of neuron and glia formation in the CNS[37], here we provide new evidence that these transcription factors also play critical role on the rate of neuron production from the MGE under normal conditions and are therefore necessary factors for generating the proper ratio of excitatory and inhibitory neurons in the neocortex.

The present analyses of Ts65Dn forebrain development provide a novel explanation of how several prenatally-specified abnormalities combine to fundamentally alter the formation and maintenance of proper cortical circuits. A complex set of prenatal defects thereby lead to the learning and memory deficits seen in Ts65Dn mice and in DS children. The results strongly suggest that widespread effects of O*lig1* and *Olig2* over-expression from early developmental stages are a main component of Ts65Dn/DS phenotypes. Thus, development of molecular tools for modulation of *Olig1* and *Olig2* transcription may be useful for ameliorating the cognitive deficits in DS. The results presented in this study can be used as biomarkers for the rational development of early interventional therapies of the cognitive impairments in DS.

METHODS

Animals

Ts65Dn and euploid B6EiC3 animals were generated by backcrossing Ts65Dn females to C57BL/6JEi X C3H/HeSnJ F1 hybrid (B6EiC3) males. The parental generation was obtained from the Jackson Laboratory (Bar Harbor, ME). Quantitative PCR (qPCR) genotyping was performed on genomic DNA extracted from tail tips[7]. *Olig1/2*$^{+/-}$ double heterozygote animals in C57BL/6J background[37] were obtained from David Anderson's laboratory and bred in our animal facility. All experiments involving animals were performed in accordance with institutional and federal guidelines. Mutant mice were genotyped using RT-PCR as described previously[37]. Ts65Dn females were crossed with *Olig1/2*$^{+/-}$ heterozygote males to generate Ts65Dn*Olig1/2*$^{+/+/-}$ animals and the mutants were genotyped using both qPCR and PCR.

Tissue processing

Ts65Dn and euploid littermates at postnatal day (P) 8, P15 and P30 were anesthetized by Forane (1-chloro-2,2,2-trifluoroethyl difluoromethyl ether) and perfused intracardially with 1M phosphate buffered saline (PBS, pH 7.4) followed by 4% paraformaldehyde (PFA). The perfused brains of the postnatal animals as well as the fresh embryonic brains were removed and fixed in PFA overnight at 4°C followed by 30% sucrose. All samples were embedded in Tissue-Tek OCT compound (Sakura Finetek Inc., Torrance, CA), frozen on dry ice and

sectioned (20 μm) by Microm HE505E cryostat (ThermoFisher Scientific, Kalamazoo, MI). All measurements and analyses were done at the level of sensorimotor cortex.

Immunohistochemistry

All immunohistochemical reactions were performed on 20μm frozen brain sections from P8, P15 and P30 pups unless otherwise stated. The antibodies used were rabbit anti-calretinin, calbindin, parvalbumin (1:1000, Chemicon, Temecula, CA), *Olig2* (1:500, Abcam, Cambridge, MA), Ki67 (1:500, Vector Laboratories, Burlingame, CA), Phospho-histone3 (PH3, 1:250, Upstate, Lake Placid, NY) and Tbr1 (1:2000, a gift from Dr. Robert Hevner, University of Washington, Seattle, WA), rat anti- somatostatin (1:250, Chemicon) and BrdU (1:100, Abcam) and mouse anti- β-tubulin III (TUJ1, 1:500, Covance, Berkeley, CA) and parvalbumin (!:500, Sigma). The secondary antibodies used were AlexaFluor 488, AlexaFluor 546 conjugated or biotinylated goat anti-rabbit, donkey anti-rat, or goat anti-mouse (1:200, Invitrogen, Carlsbad, CA). All frozen sections were mounted with Vectashield (Vector Laboratories) and paraffin sections were mounted with permount (Fisher Scientific).

Dioxygenin-labeled RNA in situ hybridization

RNA in situ hybridization was performed on E13.5 and E14.5 paraffin sections and E15.5 frozen sections for *Dlx2, Dlx5, Nkx2-1, Lhx6* and somatostatin probes. Sections were postfixed in 4% PFA for 10 min followed by 2×5 min rinses in PBS. Proteinase K (Invitrogen) digestion (20 μg/mL in PBS) was carried out for 6 min followed by 1×5 min rinse in PBS, refixing for 5 min in 4% PFA and another PBS rinse. The sections were acetylated for 10 min (2.2 g triethanolamine hydrochloride, 540 μL of 10 N NaOH, 300 μL of acetic anhydride in 60 mL of molecular grade water) prior to 3×5 min rinses in PBS. RNA probes, prepared at a dilution of 2 μL/mL of hybridization solution (50% formamide, 10% dextran sulfate, 1% 100× Denhart's, 250 μg/mL yeast tRNA, 0.3 M NaCl, 20 mM Tris–HCl, pH8, 5 mM ethylene diaminetetraacetic acid [EDTA], 10 mM $NaPO_4$, 1% sarcosyl in diethylpyrocarbonate-treated H_2O, were incubated at 80 °C for 2 min. Thereafter, 250 μL of the probe mix was applied to each slide, coverslipped with Hybri-slips (Sigma) and placed in a sealed box humidified with 50% formamide and H_2O and incubated at 55 °C overnight. The next day, the Hybri-slips were floated off by placing the slides in 5× saline-sodium citrate buffer, prior to a 30-min high stringency wash in prewarmed 50% formamide, 2× SSC at 65 °C. Next, the sections were rinsed in 3×10 min rinses in RNase buffer (0.5 M NaCl, 10 mM Tris–HCl, pH 7.5, 5 mM EDTA), followed by RNaseA (Roche, Indianapolis, IN) treatment (20 μg/mL in RNase buffer) for 30 min and one 15 min rinse in RNase buffer, all at 37 °C. The high stringency washes were repeated twice for 20 min each at 65 °C, followed by a 15 min rinse in 2× SSC, then 0.1× SSC, both at 37 °C and a PBT (PBS + 0.1% Tween 20; Sigma) rinse for 15 min at room temperature. The sections were blocked with 10% goat serum in PBT for 1 h at room temperature, prior to a 3-h incubation with an alkaline phosphatase-coupled anti-DIG antibody (1:5000 in 1% goat serum in PBT; Roche) in a humidified chamber at room temperature. Then, the sections were rinsed extensively in PBT at room temperature (4×15 min rinses) and then underwent 2×10 min rinses in freshly prepared NTMT buffer (100 mM NaCl, 100 mM Tris–HCl, pH 9.5, 50 mM $MgCl_2$, 0.1% Tween 20). The sections were then placed in a light-protected humidified

chamber with approximately 400 μL of BM-purple AP substrate (Roche) containing ~0.25 mg/mL levamisol (Sigma) until satisfactory staining was achieved, typically overnight. Finally, the sections were rinsed twice in PBS, coverslipped using Crystal mount aqueous mounting media (Sigma) and photographed immediately.

In vivo neurogenesis assay

Pregnant Ts65Dn females at E13.5 were injected once with BrdU (50 μg per gm body weight, i.p.) and killed 24 hrs (n=3) after injection. Twenty micron coronal sections of the frozen heads were stained for either BrdU and TUJ1 or BrdU and Ki67. Images with Z-stacks (1 μm steps) were collected on a confocal microscope (Zeiss LSM 510 Meta). In the images with BrdU/TUJ1 double staining, BrdU$^+$ and BrdU$^+$/TUJ1$^+$ cells were counted in the SVZ of ganglionic eminences in the ventral forebrain. We considered the BrdU$^+$/TUJ1$^+$ labeling to represent the neurons which had exited the cell cycle just after the BrdU injection. Similarly, in the images with BrdU/Ki67 double staining, BrdU$^+$ and BrdU$^+$/Ki67$^-$ cells were counted in the VZ and SVZ of the medial ganglionic eminence. The BrdU$^+$/Ki67$^-$ cells represent the cells exiting the cell cycle just after the BrdU injection.

Cell cycle analysis

A cumulative BrdU labeling protocol was followed to determine (i) the growth fraction (i.e. the proportion of cells that comprise the proliferating population), (ii) Tc, the length of the cell cycle and (iii) the time to reach the growth fraction (Tc-Ts)[7]. Pregnant Ts65Dn females at E13.5 or E14.5 were injected with BrdU (50μg per gm body weight, i.p.) every 2 hrs with survival times of 2, 6, 10, 14, 18 and 24 hrs (n=3–6 for each time point per genotype). The last injection was given 2 hrs before sacrifice. The labeling index (LI), or fraction of cells labeled with BrdU, was determined at each time point using immunohistochemistry. All labeling experiments were started at 7 AM.

Western blot analysis

For Western blot analysis, calbindin protein from the cortex of P15 pups was obtained by tissue homogenization in RIPA buffer (50mM Tris-HCl pH 7.4, 0.9% NaCl, 1% NP-40, and 0.25% sodium deoxycholate). Protein concentration was determined according to manufacturer's instruction using BCA Protein Assay Kit (Pierce, Rockford, IL). Twenty micrograms of protein homogenate were loaded per well for electrophoresis after which the proteins were transferred to polyvinylidene difluoride membranes and blocked with 5% milk for 1 hour at room temperature. The blots were incubated overnight at 4°C with rabbit anti-calbindin (1:5000, Chemicon) and mouse anti-β-actin (1:20,000, Chemicon). After washing, blots were incubated for one hour with HRP-conjugated secondary antibodies (1:10,000, Chemicon). Blots were developed by chemiluminescence using SuperSignal Kit (Pierce). Quantification of band densitometry was performed using Scion Image software.

Semi quantitative RT-PCR

Total RNAs were prepared using Trizol (Invitrogen) from the medial ganglionic eminence of euploid and Ts65Dn brain at E14.5. cDNA was synthesized from 2 μg of total RNA using ThermoScript RT-PCR system (Invitrogen). Twenty nanograms of the cDNA were used

with primers for *Olig1* and *Olig2* (target gene) and β-actin (control gene) for PCR by SYBR-Green method. The reaction was carried out at 95°C for 5 min, followed by 30 cycles of 95°C for 15 sec, 58°C for 15 sec and 72°C for 15 sec and finally 72°C for 10 min on an iCycler (BioRad, Hercules, CA) with a 96 well format. Relative quantification was calculated by Gene Expression Analysis for iCycler (BioRad).

Electrophysiology

Mice, 2–3 weeks old, were anesthetized, decapitated and the brain was rapidly removed and placed in ice cold (~4°C) cutting artificial cerebrospinal fluid (ACSF) containing (in mM): NaCl 124, KCl 3, CaCl$_2$ 2, NaH$_2$PO$_4$ 1.25, MgSO$_4$ 5, NaHCO$_3$ 26, d-glucose 10, bubbled with a mixture of 95% O$_2$/5% CO$_2$. Parasagittal slices, 400-μm thick, were cut on a Lancer Vibratome (Vibratome series 1000; Vibratome, St. Louis, Missouri USA) and transferred to a warmed (~37°C) solution of 50% slicing ACSF and 50% recording ACSF (the same composition as cutting ACSF, but MgSO$_4$ at 1 instead of 5 mM) bubbled with a mixture of 95% O$_2$/5% CO$_2$. After 20 minutes they were transferred to room temperature (~21°C) O$_2$/CO$_2$ bubbled recording ACSF where they were maintained for at least 1 hour before recording. Slices were placed in a recording chamber containing bubbled recording ACSF on the stage of an upright Zeiss FS-1 microscope (Carl Zeiss Microimaging Inc., Thornwood, NY). Using a Photonics IR camera, CA1 pyramidal neurons were identified and a whole-cell patch-clamp configuration was obtained with a borosilicate patch pipette of resistance 3–5 M containing (in mM): K-gluconate 130, KCl 15, HEPES 5, EGTA 1, Mg-ATP 4, Na-GTP 0.3 with pH adjusted to ~7.3 with KOH. Recordings were performed in voltage-clamp configuration and data acquired by way of an Axopatch 200A or 200B amplifier (Molecular Devices, Sunnyvale, CA), filtered at 5 kHz (8-pole Bessel filter, NPI, ALA Scientific Instruments, Inc., Westbury, NY, USA), and recorded on a personal computer using Clampex acquisition software (Molecular Devices). After perfusion of 20 μM CNQX and 50 μM D-APV (to block AMPA/Kainate and NMDA receptor mediated currents) sIPSC were recorded from neurons held at −70 mV under a gap free protocol and later visually inspected and detected offline using MiniAnalysis 6.0 (Synaptosoft, Decatur GA.). sIPSC were eliminated by 20 μM bicuculline (specific GABA$_A$ receptor antagonist) in both diploid (n=4) and Ts65Dn (n=5) slices indicating that events were GABA$_A$ mediated. IPSC frequency probability distributions were generated from instantaneous event frequencies pooled from all cells for each condition (euploid, n=32; Ts65Dn*Olig1/2*$^{+/+/−}$, n=27; Ts65Dn, n=34). mIPSC were also recorded at −70 mV in perfusate of 1 μM TTX (to block action potentials and thus sIPSCs), 20 μM CNQX and 50 μM D-APV and analyzed as described above for sIPSCs.

Image analysis

All fluorescent images were taken on a LSM510 Meta confocal microscope (Carl Zeiss Inc., Germany). Immunolabeled cells in each cortical layer (viz. layers II–III, IV, V and VI) were counted every tenth sections of 20 μm each (every 200 μm) in a 500μm width x 150μm height frame in 15 μm thick z-stack images (1μm steps) using Volocity (Improvision, Lexington, MA) and LSM 510 softwares packages. The layers of the neocortex were discriminated using the layer markers, Brn1 (layer I–III), RORβ (layer IV), ER81 (layer V) and Foxp2 (layer VI). The VZ and SVZ abventricular boundary in the MGE was estimated

at 100 μm. The bright field images were taken on a BX40 Olympus microscope (Olympus America Inc., Center Valley, PA) and immunolabeled cells were counted using NIH ImageJ software.

Statistical analysis

Data are presented as mean ± S.D. unless otherwise stated. Comparisons of mean differences between groups were made by unpaired two-tailed Student's *t*-test unless otherwise stated. A probability level of p<0.05 was considered to be statistically significant.

Supplementary Material

Refer to Web version on PubMed Central for supplementary material.

Acknowledgments

References

1. Epstein CJ. Developmental genetics. Experientia. 1986; 42:1117–1128. [PubMed: 3021509]

2. Korenberg JR, et al. Down syndrome: toward a molecular definition of the phenotype. Am J Med Genet Suppl. 1990; 7:91–97. [PubMed: 2149983]

3. Golden J, Hyman B. Development of the superior temporal neocortex is anomalous in trisomy 21. J Neuropathol Exp Neurol. 1994; 53:513–520. [PubMed: 8083693]

4. Schmidt-Sidor B, Wisniewski KE, Shepard TH, Sersen EA. Brain growth in Down syndrome subjects 15 to 22 weeks of gestational age and birth to 60 months. Clin Neuropathol. 1990; 9:181–190. [PubMed: 2146054]

5. Weitzdoerfer R, Dierssen M, Fountoulakis M, Lubec G. Fetal life in Down syndrome starts with normal neuronal density but impaired dendritic spines and synaptosomal structure. J Neural Transm Suppl. 2001:59–70. [PubMed: 11771761]

6. Baxter LL, Moran TH, Richtsmeier JT, Troncoso J, Reeves RH. Discovery and genetic localization of Down syndrome cerebellar phenotypes using the Ts65Dn mouse. Hum Mol Genet. 2000; 9:195–202. [PubMed: 10607830]

7. Chakrabarti L, Galdzicki Z, Haydar TF. Defects in embryonic neurogenesis and initial synapse formation in the forebrain of the Ts65Dn mouse model of Down syndrome. J Neurosci. 2007; 27:11483–11495. [PubMed: 17959791]

8. Lorenzi HA, Reeves RH. Hippocampal hypocellularity in the Ts65Dn mouse originates early in development. Brain Res. 2006; 1104:153–159. [PubMed: 16828061]

9. Belichenko PV, et al. Excitatory-inhibitory relationship in the fascia dentata in the Ts65Dn mouse model of Down syndrome. J Comp Neurol. 2009; 512:453–466. [PubMed: 19034952]

10. Belichenko PV, et al. Synaptic structural abnormalities in the Ts65Dn mouse model of down syndrome. J Comp Neurol. 2004; 480:281–298. [PubMed: 15515178]

11. Kleschevnikov AM, et al. Hippocampal long-term potentiation suppressed by increased inhibition in the Ts65Dn mouse, a genetic model of Down syndrome. J Neurosci. 2004; 24:8153–8160. [PubMed: 15371516]

12. Siarey RJ, Stoll J, Rapoport SI, Galdzicki Z. Altered long-term potentiation in the young and old Ts65Dn mouse, a model for Down Syndrome. Neuropharmacology. 1997; 36:1549–1554. [PubMed: 9517425]

13. Costa AC, Walsh K, Davisson MT. Motor dysfunction in a mouse model for Down syndrome. Physiol Behav. 1999; 68:211–220. [PubMed: 10627083]

14. Hyde LA, Frisone DF, Crnic LS. Ts65Dn mice, a model for Down syndrome, have deficits in context discrimination learning suggesting impaired hippocampal function. Behav Brain Res. 2001; 118:53–60. [PubMed: 11163633]

15. Reeves RH, et al. A mouse model for Down syndrome exhibits learning and behaviour deficits. Nat Genet. 1995; 11:177–184. [PubMed: 7550346]

16. Kurt MA, Davies DC, Kidd M, Dierssen M, Florez J. Synaptic deficit in the temporal cortex of partial trisomy 16 (Ts65Dn) mice. Brain Res. 2000; 858:191–197. [PubMed: 10700614]

17. Perez-Cremades D, et al. Alteration of inhibitory circuits in the somatosensory cortex of Ts65Dn mice, a model for Down's syndrome. J Neural Transm.

18. Costa AC, Grybko MJ. Deficits in hippocampal CA1 LTP induced by TBS but not HFS in the Ts65Dn mouse: a model of Down syndrome. Neurosci Lett. 2005; 382:317–322. [PubMed: 15925111]

19. Fernandez F, et al. Pharmacotherapy for cognitive impairment in a mouse model of Down syndrome. Nat Neurosci. 2007; 10:411–413. [PubMed: 17322876]

20. Haydar TF. Advanced microscopic imaging methods to investigate cortical development and the etiology of mental retardation. Ment Retard Dev Disabil Res Rev. 2005; 11:303–316. [PubMed: 16240412]

21. Miller MW. Cogeneration of retrogradely labeled corticocortical projection and GABA-immunoreactive local circuit neurons in cerebral cortex. Brain Res. 1985; 355:187–192. [PubMed: 3910166]

22. Valcanis H, Tan SS. Layer specification of transplanted interneurons in developing mouse neocortex. J Neurosci. 2003; 23:5113–5122. [PubMed: 12832535]

23. DeFelipe J. Neocortical neuronal diversity: chemical heterogeneity revealed by colocalization studies of classic neurotransmitters, neuropeptides, calcium-binding proteins, and cell surface molecules. Cereb Cortex. 1993; 3:273–289. [PubMed: 8104567]

24. Kawaguchi Y, Kubota Y. GABAergic cell subtypes and their synaptic connections in rat frontal cortex. Cereb Cortex. 1997; 7:476–486. [PubMed: 9276173]

25. Markram H, et al. Interneurons of the neocortical inhibitory system. Nat Rev Neurosci. 2004; 5:793–807. [PubMed: 15378039]

26. Wonders CP, Anderson SA. The origin and specification of cortical interneurons. Nat Rev Neurosci. 2006; 7:687–696. [PubMed: 16883309]

27. Hobert O, Westphal H. Functions of LIM-homeobox genes. Trends Genet. 2000; 16:75–83. [PubMed: 10652534]

28. Liodis P, et al. Lhx6 activity is required for the normal migration and specification of cortical interneuron subtypes. J Neurosci. 2007; 27:3078–3089. [PubMed: 17376969]

29. Shirasaki R, Pfaff SL. Transcriptional codes and the control of neuronal identity. Annu Rev Neurosci. 2002; 25:251–281. [PubMed: 12052910]

30. Eisenstat DD, et al. DLX-1, DLX-2, and DLX-5 expression define distinct stages of basal forebrain differentiation. J Comp Neurol. 1999; 414:217–237. [PubMed: 10516593]

31. Grigoriou M, Tucker AS, Sharpe PT, Pachnis V. Expression and regulation of Lhx6 and Lhx7, a novel subfamily of LIM homeodomain encoding genes, suggests a role in mammalian head development. Development. 1998; 125:2063–2074. [PubMed: 9570771]

32. Porteus MH, Bulfone A, Ciaranello RD, Rubenstein JL. Isolation and characterization of a novel cDNA clone encoding a homeodomain that is developmentally regulated in the ventral forebrain. Neuron. 1991; 7:221–229. [PubMed: 1678612]

33. Sussel L, Marin O, Kimura S, Rubenstein JL. Loss of Nkx2.1 homeobox gene function results in a ventral to dorsal molecular respecification within the basal telencephalon: evidence for a transformation of the pallidum into the striatum. Development. 1999; 126:3359–3370. [PubMed: 10393115]

34. Alifragis P, Liapi A, Parnavelas JG. Lhx6 regulates the migration of cortical interneurons from the ventral telencephalon but does not specify their GABA phenotype. J Neurosci. 2004; 24:5643–5648. [PubMed: 15201337]

35. Lu QR, et al. Common developmental requirement for Olig function indicates a motor neuron/ oligodendrocyte connection. Cell. 2002; 109:75–86. [PubMed: 11955448]

36. Takebayashi H, et al. Dynamic expression of basic helix-loop-helix Olig family members: implication of Olig2 in neuron and oligodendrocyte differentiation and identification of a new member, Olig3. Mech Dev. 2000; 99:143–148. [PubMed: 11091082]

37. Zhou Q, Anderson DJ. The bHLH transcription factors OLIG2 and OLIG1 couple neuronal and glial subtype specification. Cell. 2002; 109:61–73. [PubMed: 11955447]

38. Bertrand N, Castro DS, Guillemot F. Proneural genes and the specification of neural cell types. Nat Rev Neurosci. 2002; 3:517–530. [PubMed: 12094208]

39. Ma Q. Transcriptional regulation of neuronal phenotype in mammals. J Physiol. 2006; 575:379–387. [PubMed: 16825304]

40. Miyoshi G, Butt SJ, Takebayashi H, Fishell G. Physiologically distinct temporal cohorts of cortical interneurons arise from telencephalic Olig2-expressing precursors. J Neurosci. 2007; 27:7786–7798. [PubMed: 17634372]

41. Kahlem P, et al. Transcript level alterations reflect gene dosage effects across multiple tissues in a mouse model of down syndrome. Genome Res. 2004; 14:1258–1267. [PubMed: 15231742]

42. Contestabile A, et al. Cell cycle alteration and decreased cell proliferation in the hippocampal dentate gyrus and in the neocortical germinal matrix of fetuses with down syndrome and in Ts65Dn mice. Hippocampus. 2007

43. Segal DJ, McCoy EE. Studies on Down's syndrome in tissue culture. I. Growth rates and protein contents of fibroblast cultures. J Cell Physiol. 1974; 83:85–90. [PubMed: 4273197]

44. Clark S, Schwalbe J, Stasko MR, Yarowsky PJ, Costa AC. Fluoxetine rescues deficient neurogenesis in hippocampus of the Ts65Dn mouse model for Down syndrome. Exp Neurol. 2006; 200:256–261. [PubMed: 16624293]

45. Freund TF, Buzsaki G. Interneurons of the hippocampus. Hippocampus. 1996; 6:347–470. [PubMed: 8915675]

46. Dierssen M, et al. Alterations of neocortical pyramidal cell phenotype in the Ts65Dn mouse model of Down syndrome: effects of environmental enrichment. Cereb Cortex. 2003; 13:758–764. [PubMed: 12816891]

47. Gibson JR, Bartley AF, Hays SA, Huber KM. Imbalance of neocortical excitation and inhibition and altered UP states reflect network hyperexcitability in the mouse model of fragile X syndrome. J Neurophysiol. 2008; 100:2615–2626. [PubMed: 18784272]

48. Polleux F, Lauder JM. Toward a developmental neurobiology of autism. Ment Retard Dev Disabil Res Rev. 2004; 10:303–317. [PubMed: 15666334]

49. Cortez MA, et al. Infantile Spasms and Down syndrome: A New Animal Model. Pediatr Res. 2009

50. Harashima C, et al. Abnormal expression of the G-protein-activated inwardly rectifying potassium channel 2 (GIRK2) in hippocampus, frontal cortex, and substantia nigra of Ts65Dn mouse: a model of Down syndrome. J Comp Neurol. 2006; 494:815–833. [PubMed: 16374808]
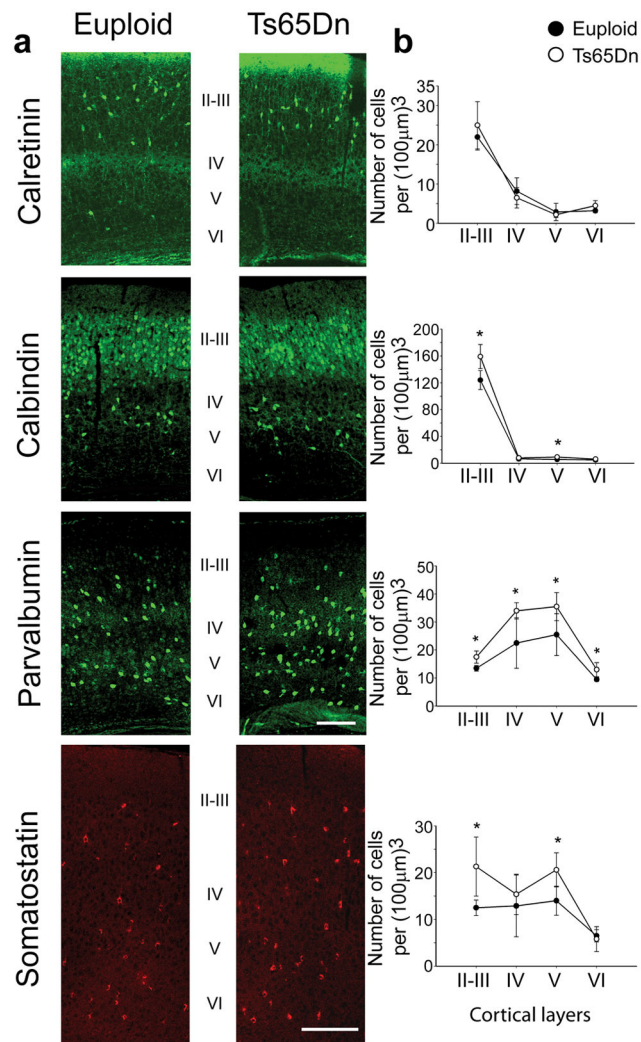
Figure 1. Preferential over-production of a subset of interneurons in Ts65Dn neocortex
(**a**) Brain sections of P15 Ts65Dn and euploid littermates were immunostained for different interneuron markers (viz. Calretinin, Calbindin, Parvalbumin and Somatostatin). Cell counts were performed within a fixed area (500μmx150μm) for all the different layers of the cortex. The layer boundaries were determined using molecular layer markers. (**b**) Comparing the number of calretinin, calbindin, somatostatin and parvalbumin positive cells at this postnatal developmental time point demonstrated a significant increase in calbindin, somatostatin and parvalbumin expressing cells in Ts65Dn cortex with no change in calretinin+ cells. Data points represent mean ± s.d. (n=6 mice for each age and group). *p<0.02 by unpaired two-tailed *t*-test. Scale bars, 100 μm. See Supplementary Fig. 2 online for analyses at other ages.
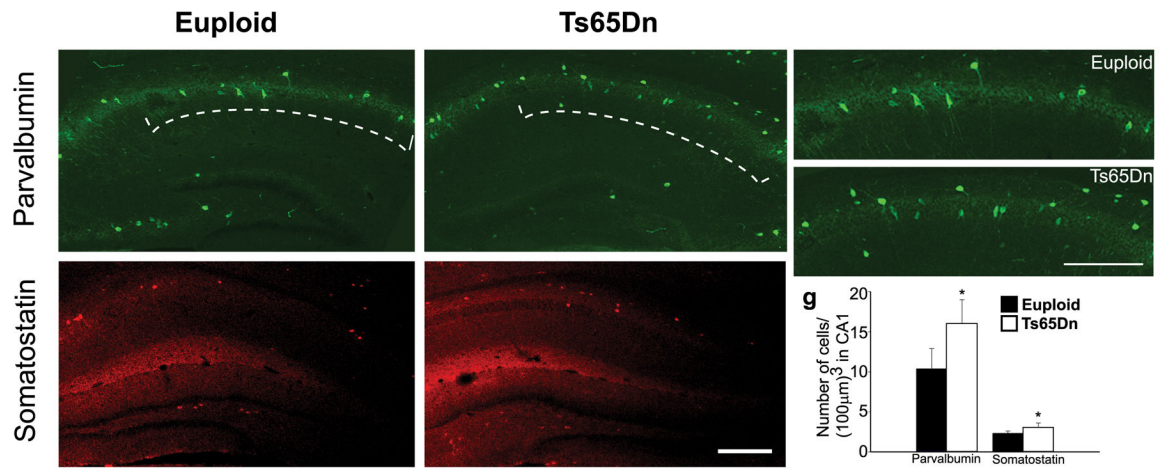
Figure 2. Over-production of a subset of interneurons in Ts65Dn hippocampus
(**a, b**) Confocal images of parvalbumin expressing cells in the Ts65Dn and euploid
hippocampus at P15. (**e**, **f**) Higher magnification of parvalbumin$^+$ cells in the CA1 region of
the Ts65Dn and euploid hippocampus. (**c**, **d**) Confocal images of somatostatin expressing
cells in the Ts65Dn and euploid hippocampus at P15. (**g**) Analysis of cell counting
uncovered an overabundance of parvalbumin and somatostatin-expressing inhibitory
interneurons in the Ts65Dn brain. This is a phenocopy of the results in the Ts65Dn
neocortical wall (Figure 1) and implicates changes in production of these specific
interneuron subtypes. Data points represent mean ± s.d. (n=4 mice for each age and group).
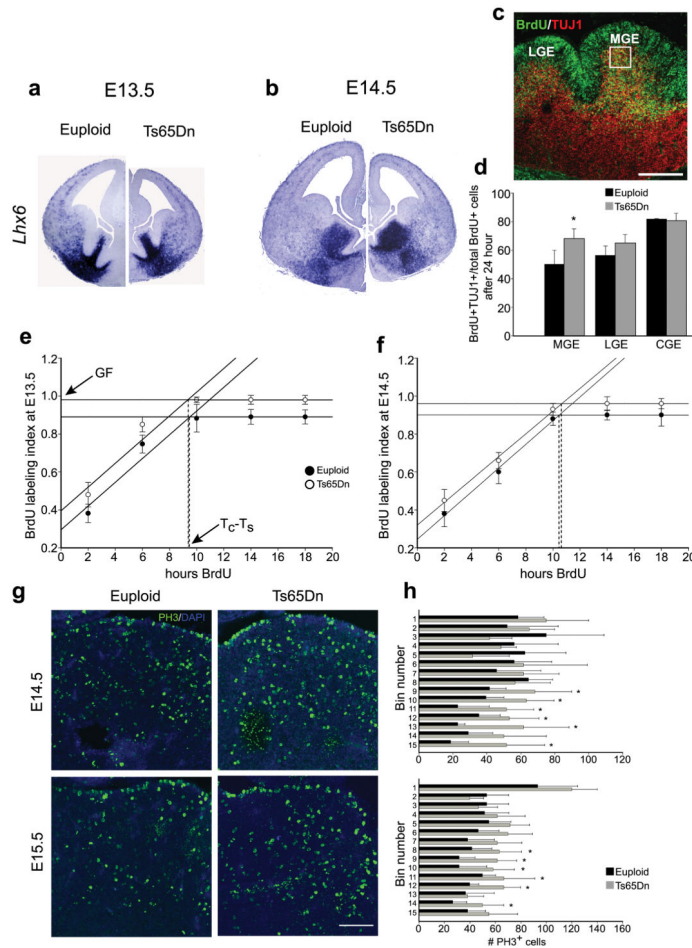*p<0.05 by unpaired two-tailed *t*-test. Scale bars, 200 μm.

Figure 3. Increased gene expression and proliferation in the MGE of the Ts65Dn ventral telencephalon

(**a, b**) *Lhx6* expression was increased in the MGE of Ts65Dn brain at E13.5 and E14.5. Scale bar, 200 μm. See Supplementary figure 5 for additional markers. (**c, d**) E13.5 timed pregnant Ts65Dn females were injected (intraperitoneally) with BrdU to label a cohort of neural progenitors in S-phase and embryos were harvested 24 h later. (**c**) A representative section stained with antibodies to BrdU (green) and TUJ1 (red). Scale bar, 200 μm. (**d**) The fraction of cells labeled with both BrdU and TUJ1 (BrdU$^+$/TUJ1$^+$; newly generated neurons) 24 h after pulse label is 36% higher in the MGE of Ts65Dn. No significant change in LGE or CGE neurogenesis was observed in Ts65Dn brains, suggesting that increased neurogenesis was specific to the Ts65Dn MGE during this period of time. (**e, f**) The cumulative labeling plots for MGE progenitors at E13.5 and E14.5 demonstrate that the labeling index (percentage of BrdU$^+$ cells) rises precipitously until reaching saturation at the GF value, which represents the proportion of the precursor cells that are participating in the cell cycle. The time to reach saturation defines the T_c-T_s value, which was normal in Ts65Dn (see also Supplementary Table 2). (**g, h**) Distribution of PH3-labeled M-phase cells in the MGE at E14.5 and E15.5. Starting from the ventricular border, the MGE was divided into 15 bins each 20 μm in thickness. Scale bar, 100 μm. The number of mitotic cells in the SVZ of Ts65Dn MGE was increased compared to euploid indicating an increase in

abventricular mitoses in Ts65Dn. Data points represent mean ± s.d. (n=3–6 mice for each age and group). *p<0.05; by unpaired two-tailed *t*-test.
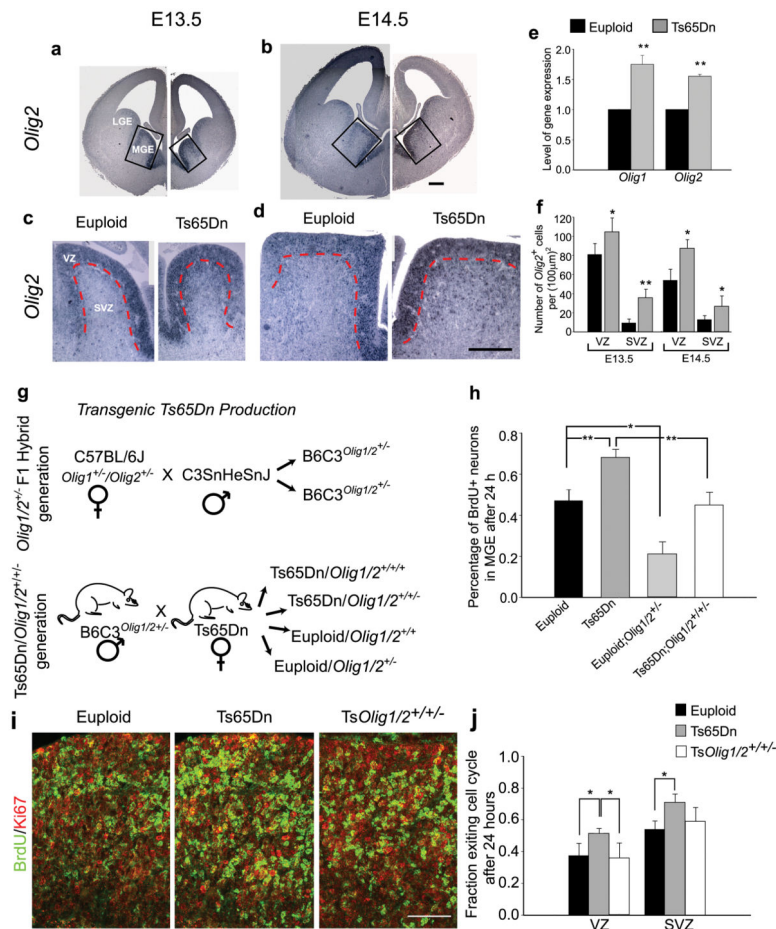
Figure 4. Normalization of *Olig* genes rescues the neurogenesis phenotype in Ts65Dn*Olig1/2*$^{+/+/-}$ (Ts*Olig1/2*$^{+/+/-}$) MGE

(**a, b**) *Olig2* expression was increased in the MGE of Ts65Dn brain at E13.5 and E14.5. Higher magnification shows an increased number of *Olig2* expressing cells in the MGE of Ts65Dn mice at E13.5 (**c**) and E14.5 (**d**). Scale bar, 200 μm. (**e**) Semi quantitative RT-PCR indicates higher expression of *Olig1* and *Olig2* genes in the MGE of Ts65Dn at E14.5. (**f**) Quantification of *Olig2* expressing cells demonstrates an increase in the number of *Olig2*$^+$ cells in the VZ and SVZ of Ts65Dn MGE compared to euploid littermates at E13.5 and E14.5. (**g**) Substitution of C57BL/6J *Olig1/2*$^{+/-}$ females for the C57BL/6JEi females yields B6C3$^{Olig1/2+/-}$ males for crossing with Ts65Dn females. Thus, the resulting Ts65Dn*Olig1/2*$^{+/+/-}$ (Ts*Olig1/2*$^{+/+/-}$), Ts65Dn*Olig1/2*$^{+/+/+}$ (Ts65Dn) and euploid pups have identical background strain potential compared to the normal Ts65Dn production techniques. We compared Ts*Olig1/2*$^{+/+/}$, Ts65Dn and euploid*Olig1/2*$^{+/+}$ littermate pups to remove any strain and construct-dependent effects on neuronal population and differentiation. (**h**) The increase in MGE neurogenesis found in Ts65Dn is prevented in Ts*Olig1/2*$^{+/+/-}$ animals at E14.5. Moreover, reduced neurogenesis was found in the MGE of euploid heterozygotes (euploid*Olig1/2*$^{+/-}$), suggesting that normal ventral telencephalic neurogenesis is dependent on *Olig1* and *Olig2* gene copy number and expression. (**i, j**) To determine the q-fraction 24 h after BrdU injection, sections from euploid, Ts65Dn and Ts*Olig1/2*$^{+/+/-}$ brains were stained with antibodies to Ki67 (red) and BrdU (green). Scale

bar, 50 µm. The fraction of cells labeled only with BrdU (BrdU$^+$/Ki67$^-$; no longer dividing) after 24 h period (q-fraction) is higher in Ts65Dn MGE compared to euploid. However, the q-fraction increase found in Ts65Dn MGE is corrected in Ts*Olig1/2*$^{+/+/-}$ animals. Data points represent mean ± s.d. (n=3–4 mice for each age and group). *p<0.05; **p<0.005 by two-tailed *t*-test.
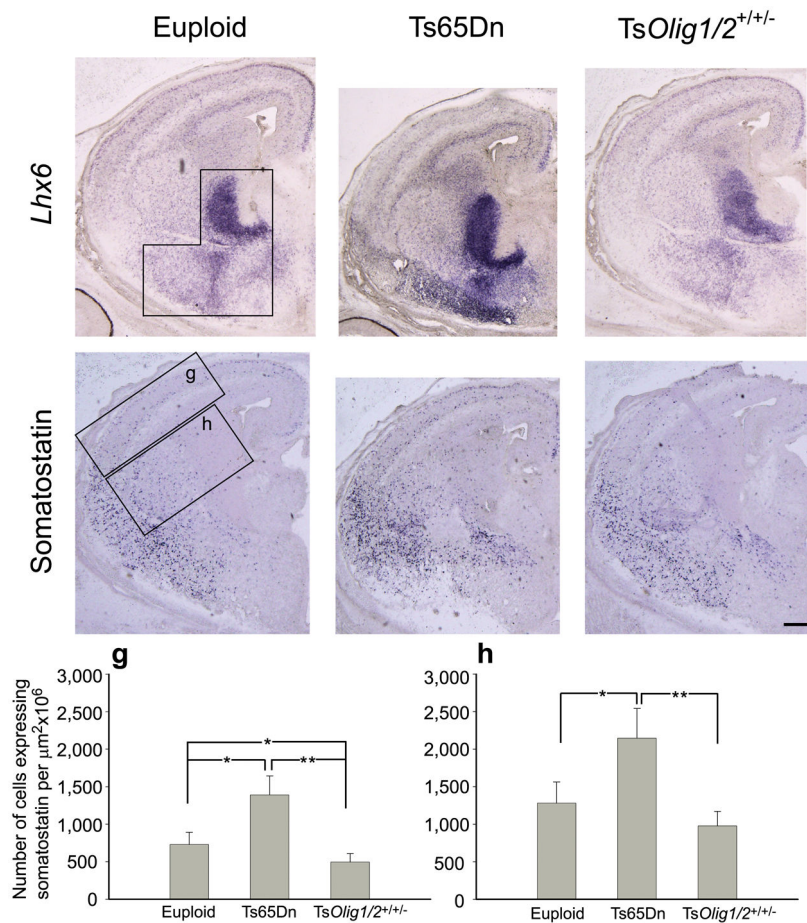
Figure 5. Gene dosage reduction rescues inhibitory neuron phenotype in embryonic Ts*Olig1/2*$^{+/+/-}$ telencephalon

(**a–f**) Postmitotic interneuron markers *Lhx6* and somatostatin were analyzed in brain sections of E15.5 euploid, Ts65Dn and Ts*Olig1/2*$^{+/+/-}$ embryos by *in situ* hybridization. (**a–c**) The *Lhx6* expression pattern in Ts*Olig1/2*$^{+/+/-}$ MGE is similar to euploid. (**d–f**) Somatostatin expression in Ts*Olig1/2*$^{+/+/-}$ telencephalon is comparable to euploid. The boxed areas **g** and **h** represent the cell counting areas for dorsal and ventral telencephalon respectively. (**g, h**) Comparing the number of somatostatin-expressing cells demonstrates an increase in Ts65Dn telencephalon while the Ts*Olig1/2*$^{+/+/-}$ rescued animals exhibited a normal number of somatostatin-expressing cells in dorsal telencephalon and no significant difference in the ventral telencephalon. Data points represent mean ± s.d. (n=3 mice for each age and group). *p<0.05; **p<0.005 by unpaired two-tailed *t*-test. Scale bar: 200 μm.
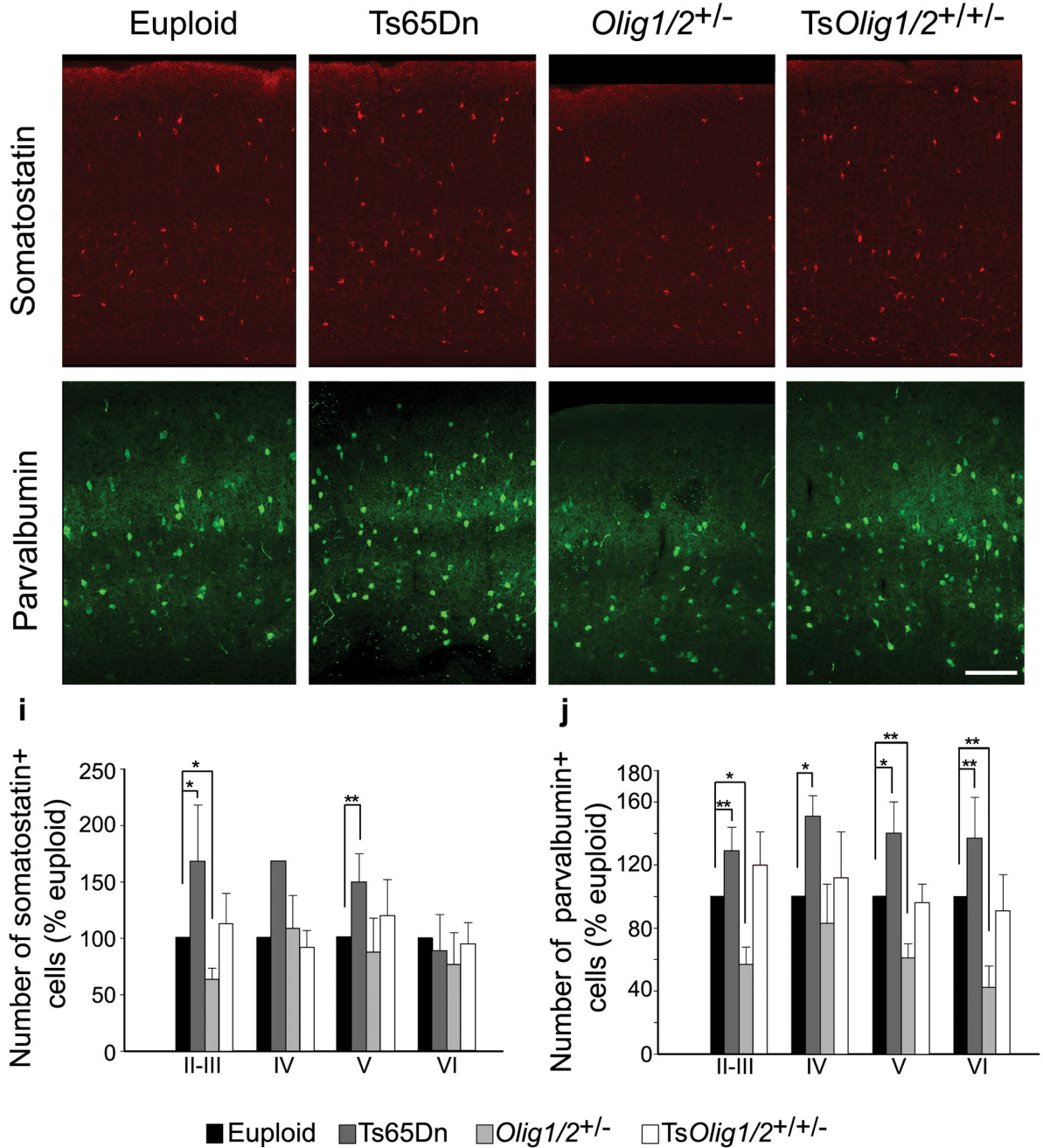
Figure 6. Normal number of inhibitory neurons in postnatal Ts*Olig1/2*$^{+/+/-}$ neocortex
(**a–d**) Confocal images of somatostatin expressing cells in the neocortex of Ts65Dn, euploid, euploid*Olig1/2*$^{+/-}$ and Ts*Olig1/2*$^{+/+/-}$ littermates at P15. (**e–h**) Confocal images of parvalbumin expressing cells in the neocortex of the same animals. Immunoreactive cells were counted within a fixed area (500μmx150μm) for all the different layers of the cortex. The layer boundaries were determined using molecular layer markers. (**i–j**) Comparing the number of somatostatin and parvalbumin positive cells demonstrates that the increased interneuron phenotype in Ts65Dn neocortex is prevented in Ts*Olig1/2*$^{+/+/-}$ animals. Moreover, significantly reduced numbers of somatostatin and parvalbumin expressing cells

were observed in the cortical layer II–III of euploid*Olig1/2*$^{+/-}$ heterozygotes. Data points represent mean ± s.e.m. (n=4–6 mice for each age and group). *p<0.05; **p<0.01 by two-tailed *t*-test. Scale bar: 100 μm.
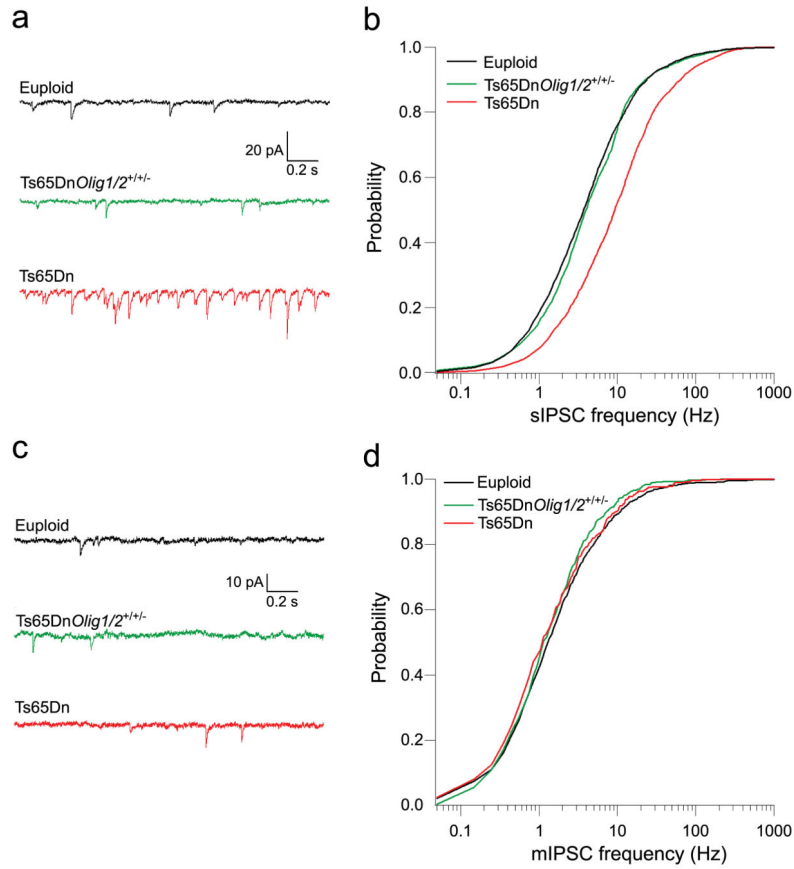
Figure 7. Reduction in *Olig1* and *Olig2* gene-dosage rescues the electrophysiological phenotype in Ts65Dn CA1 pyramidal cells

(**a**) Representative voltage clamp recordings showing increased sIPSC rates in Ts65Dn CA1 pyramidal neurons (bottom) compared to those from both euploid (top) and Ts*Olig1/2$^{+/+/-}$* (middle). (**b**) The cumulative probability distribution function for the intervals between sIPSC is shifted rightward for Ts65Dn CA1 pyramidal cells. In contrast, the curves for Ts*Olig1/2$^{+/+/-}$* and euploid mice are similar. (**c**) In the presence of TTX, IPSC rates are similar in CA1 pyramidal neurons from all mice. (**d**) The cumulative probability distribution functions for each genotype in the presence of TTX are similar.